Morphology Evolution in Nanoscale Light-Emitting Domains in MEH-PPV/PMMA Blends

Nisha A. Iyengar, Benjamin Harrison, Randolph S. Duran, Kirk S. Schanze, and John R. Reynolds*

Center for Macromolecular Science and Engineering, Department of Chemistry, University of Florida, Gainesville, Florida 32611-7200

Received July 1, 2003; Revised Manuscript Received September 19, 2003

ABSTRACT: The compositional evolution of the morphology of blends of a light-emitting conjugated polymer MEH-PPV [MEH-PPV = poly(2-methoxy-5-(2′-ethylhexyloxy)-*p*-phenylenevinylene)] with poly(methyl methacrylate) (PMMA) on a PEDOT/PSS [PEDOT/PSS = poly(3,4-ethylenedioxythiophene)/poly(styrenesulfonate)] coated glass substrate is reported. Results of AFM (topographic and phase images), optical microscopy, fluorescence microscopy, and photographs of the emission from light-emitting devices (LEDs) illustrate this morphological evolution. The 5 wt % compositional study demonstrates the stability of morphology for the blend films dried in air, vacuum-dried at room temperature, and vacuum-dried at 80 °C. Annealing above the T_g (106 °C) of PMMA caused significant dewetting between the blend and the PEDOT/PSS. At low MEH-PPV compositions, isolated light-emitting domains ranging in diameter from 300 to 900 nm and ∼100 nm in thickness were observed. At approximately 50 wt % MEH-PPV, a phase inversion was observed and a bicontinuous morphology evolved. The highest efficiency LEDs were obtained at 75 wt % MEH-PPV where a continuous light-emitting polymer structure exists surrounding isolated domains of PMMA.

Introduction

Since the discovery of light-emitting devices (LEDs) based on conjugated polymers in the 1990s,[1,2] the field has matured rapidly to the point where long-lived PLEDs can be prepared across the full visible spectrum and have reached commercial availability.[3−5] One attractive feature of these polymers is the ability to form thin films from solution by spin-coating, avoiding the need for high-vacuum deposition and allowing devices to be constructed on flexible substrates. To improve device performance, a significant amount of research has been dedicated to understand the underlying science behind the enhancement of device efficiencies and overcoming device degradation.

One area of emphasis has been the control of phase separation and morphology in polymer/polymer blends and block copolymers in which at least one of the components is a conjugated polymer. This field, which has been investigated to a limited extent, suggests possibilities for ultimate patterning and control of the color in light-emitting domains. Various copolymers including A−B block copolymers,[6] and segmented block copolymers,[7] have been used and shown to provide versatility relative to homopolymers in attempts to improve or tune a desired property. For example, PPV copolymers containing alternating aromatic conjugated and aliphatic nonconjugated blocks[8−11] were shown to have better film-forming properties and lower onset voltages than the homopolymers alone. Copolymers have been utilized to obtain efficient[12,13] blue emission by using defined conjugation lengths leading to higher band gap polymers and also have been found to improve the efficiency[14,15] of the devices.

In the case of polymer/polymer blends,[16,17] an alkyl-derivatized polythiophene (PTOPT) and PMMA have been used to create "nano-LEDs" with emitting domains on the order of 300−500 nm in diameter. The benefits and possibilities of such small light-emitting domains include using them as light sources in scanning near-field optical microscopes (SNOMs) where it is important to have small light sources, along with the possibility of using photopatterning processes to create a large number of identical patterns simultaneously. Furthermore, these polymer blends may be designed to reduce the amount of costly conjugated polymer by using a compositional majority of simple commodity polymers, resulting in considerable cost savings.

These two-phase polymer blends consist of a host−guest system. The host matrix, or the major component, can be an inert polymer like polystyrene[18] or poly(methyl methacrylate)[16] or a charge transport active polymer such as poly(vinylcarbazole).[19,20] The guest, or the minority component, is generally the light-emitting conjugated polymer. Further work in polymer blends has demonstrated that colors can be varied as a function of voltage,[21,22] and combinations of polymers with blue, red, and green emission can be used to obtain a white light-emitting diode.[23,24] Polymer blends also provide a platform with which to combine two polymers with different properties, such as hole transport or emission efficiencies with each other as opposed to preparing a multilayer device.[25] Additionally, polymer blending can be used as a tool to increase the efficiency of devices[26−28] by improving charge injection[29] and trapping. Energy transfer between the components in polymer blends leads to an enhancement in the PL efficiency of films and EL efficiency in resultant devices.[30−33] The morphology of conjugated polymer containing blends[34−37] has been characterized for a variety of systems. Domain size has been shown to be a function of both the solvent and the temperature[38] used for drying and annealing the films. Further, the operating voltages and currents in LEDs were affected by the extent of phase separation. Turning to the specific MEH-PPV/PMMA system, Chuang et al.[39] have carried out a limited study of the EL characteristics of LEDs constructed with two composi-

10.1021/ma034908w CCC: $25.00
Published on Web 11/07/2003

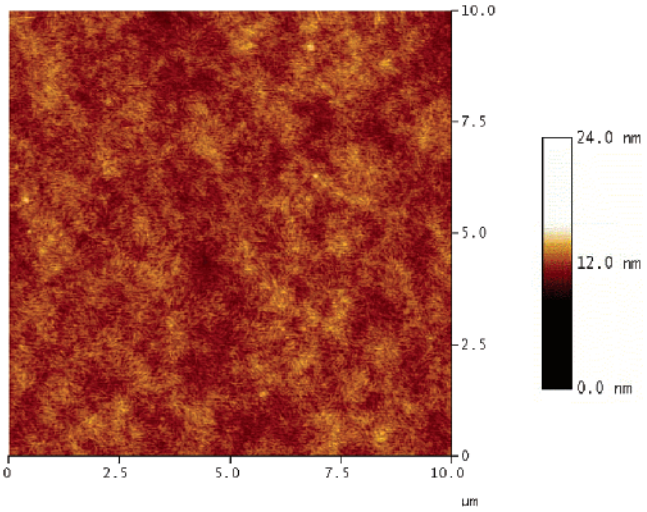

Figure 1. Topographic AFM image of MEH-PPV on PEDOT/PSS coated glass slide.

tions of MEH-PPV/PMMA and suggested that the onset voltage decreased using the blend relative to MEH-PPV alone. In this study, no enhancement in EL efficiency was observed.

Here, we report a full study of the compositional dependence of MEH-PPV/PMMA blends showing an evolution of the microstructure from isolated light-emitting domains ranging in diameter from 300 to 900 nm and ~100 nm thickness to a continuous light-emitting material. A "phase inversion" is observed at approximately 50 wt % MEH-PPV, where a bicontinuous network of the two polymers is observed. Results of AFM (topographic and phase images), optical microscopy, fluorescence microscopy, and the emission from LEDs observed using the fluorescence microscope illustrate this morphological evolution. This work demonstrates that the highest efficiency devices are obtained at 75 wt % MEH-PPV where a continuous light-emitting polymer structure exists surrounding isolated domains of PMMA.

Results and Discussion

The main focus of the research reported here is to demonstrate the effect that polymer blend composition and morphology have on the light-emitting characteristics of MEH-PPV/PMMA blends. In PLEDs, interfaces play a crucial role, as hole injection at the anode (often PEDOT/PSS coated ITO) and electron injection at the low work function metal cathode are required in order to form the emitting excited state. As such, all of the investigations reported here are carried out on polymer blend films, which have been spin-coated onto a thin layer of PEDOT/PSS (ca. 45 nm) on cleaned glass. PEDOT/PSS is commonly used as a hole-injecting and buffer layer in between the ITO anode and light-emitting polymer films. The light-emitting films develop their morphology on the PEDOT/PSS, and thus this morphology is equivalent to that obtained in the LEDs themselves. Examination of the pristine glass, ITO/glass used in device construction, and PEDOT/PSS-coated substrates with optical microscopy and AFM shows a featureless surface morphology to below 100 nm resolution. After drying the PEDOT/PSS films at 150 °C under vacuum, polymer blend solutions of varied ratios of MEH-PPV/PMMA having a combined concentration of 5.2 mg/mL total polymer were spin-coated.

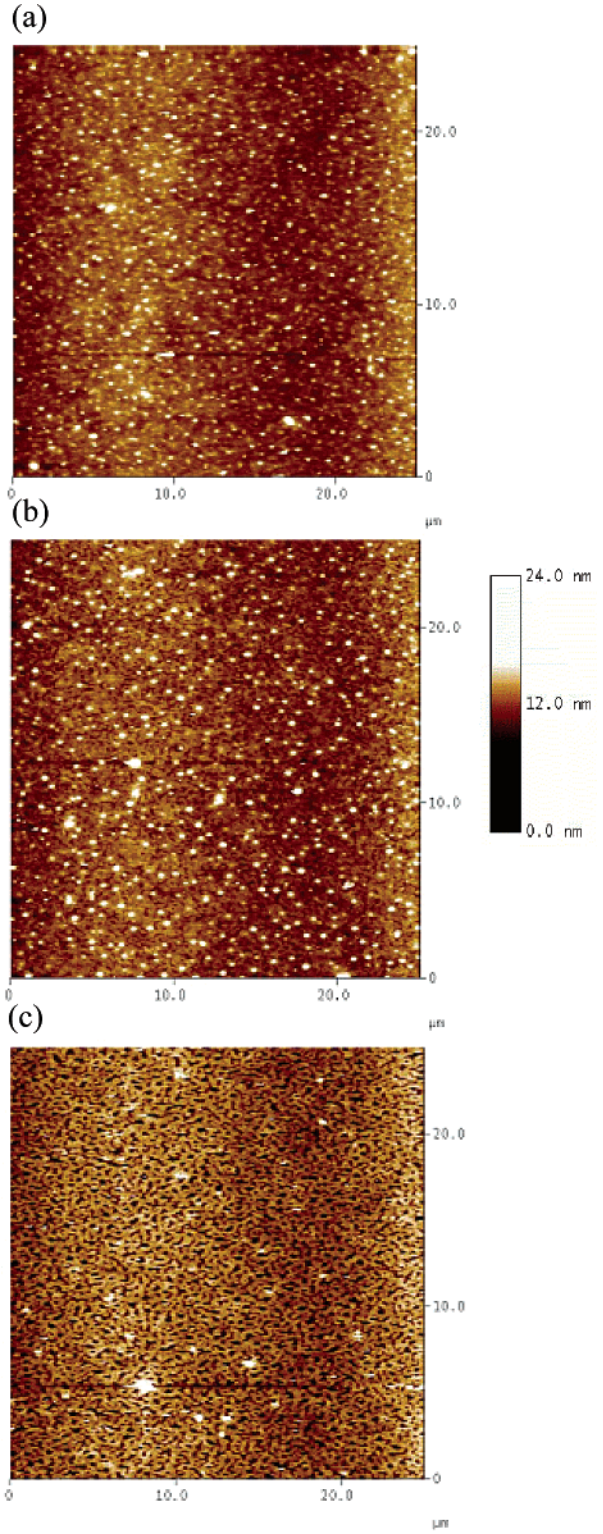

Figure 2. Topographic AFM images of 5 wt % MEH-PPV in PMMA dried (a) under vacuum, (b) at 80 °C under vacuum, and (c) at 120 °C under vacuum.

Examination of films of neat PMMA and MEH-PPV alone by AFM showed no discrete morphological features to below 100 nm. The results of Figure 1 demonstrate this as a 10 μm AFM scan of MEH-PPV exhibits a low surface roughness (R_{ms}) of ~1.0 nm. A continuous emission across the entire surface of the MEH-PPV is observed by photoluminescence (PL).

MEH-PPV/PMMA Blend Morphology. Incorporation of 5 wt % MEH-PPV in PMMA leads to distinct

Scheme 1

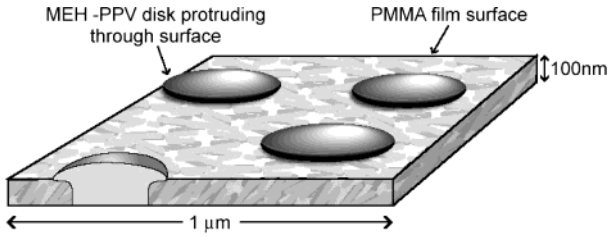

phase-separated domains of light-emitting polymer in the insulating polymer matrix as shown in Figure 2. These domains range in size from 300 to 400 nm in diameter. As the thickness of the MEH-PPV and blend films range from 100 to 120 nm, these phase-separated domains represent nanosized disks of light-emitting polymer dispersed in the insulating PMMA matrix. This morphology, as depicted by the illustration of Scheme 1, demonstrates how the MEH-PPV domains emerge from the surface of the PMMA matrix. The miscibility of the two polymers depends on the free energy of mixing, which in turn depends on both enthalpic and entropic contributions. For most binary polymer mixtures, the entropy of mixing is small, leaving the enthalpic factor as determining. The unfavorable enthalpic interaction leads to phase separation of polymer blends and gives rise to structure in the nano- and microscale. While certainly of fundamental interest, these laterally segregated domains have implications for reducing the content of precious emitting polymer in a device, controlling the emission color, as light sources for scanning-near-field optical microscopes (SNOMs) and quantum dot formation.[40]

The 5 wt % compositional study was used to demonstrate the stability of this morphology, as identical structures were observed for the blend film dried in air, vacuum-dried at room temperature (Figure 2a), and vacuum-dried at 80 °C (Figure 2b). Heating the film at 120 °C under vacuum, a temperature above glass transition temperature of the PMMA matrix (T_g = 106 °C), led to distinct morphological changes as shown in Figure 2c. It can be seen that above the T_g of PMMA a spontaneous dewetting of the PEDOT/PSS by the PMMA[41,42] occurs, leading to the formation of pinholes (small black features in the micrograph) in the film. For this reason, all of the films subsequently prepared were vacuum-dried at a temperature less than the glass transition temperature of PMMA.

The evolution of film morphology as MEH-PPV concentration is increased from 10 to 75 wt % is shown in Figures 3−6. Figure 3a,b shows the AFM topographic and phase images for blends with 10 wt % MEH-PPV. The phase-separated domains increase in size to about 500−800 nm when compared to the 5 wt % MEH-PPV

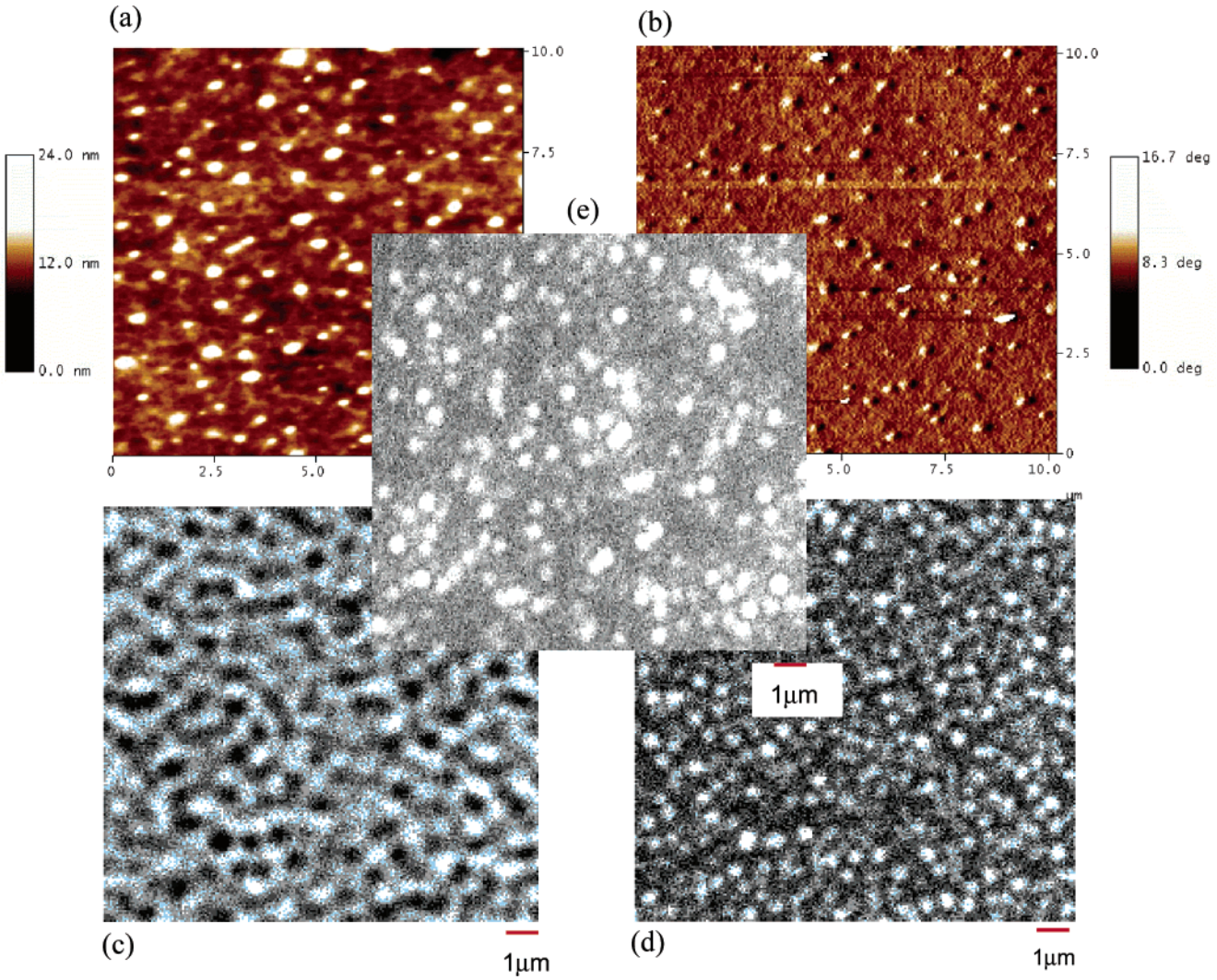

Figure 3. Images of 10 wt % MEH-PPV in PMMA: tapping mode AFM topographic (a) and phase (b) images; bright field (c) and photoluminescence (d) microscope images; (e) electroluminescence microscope image.

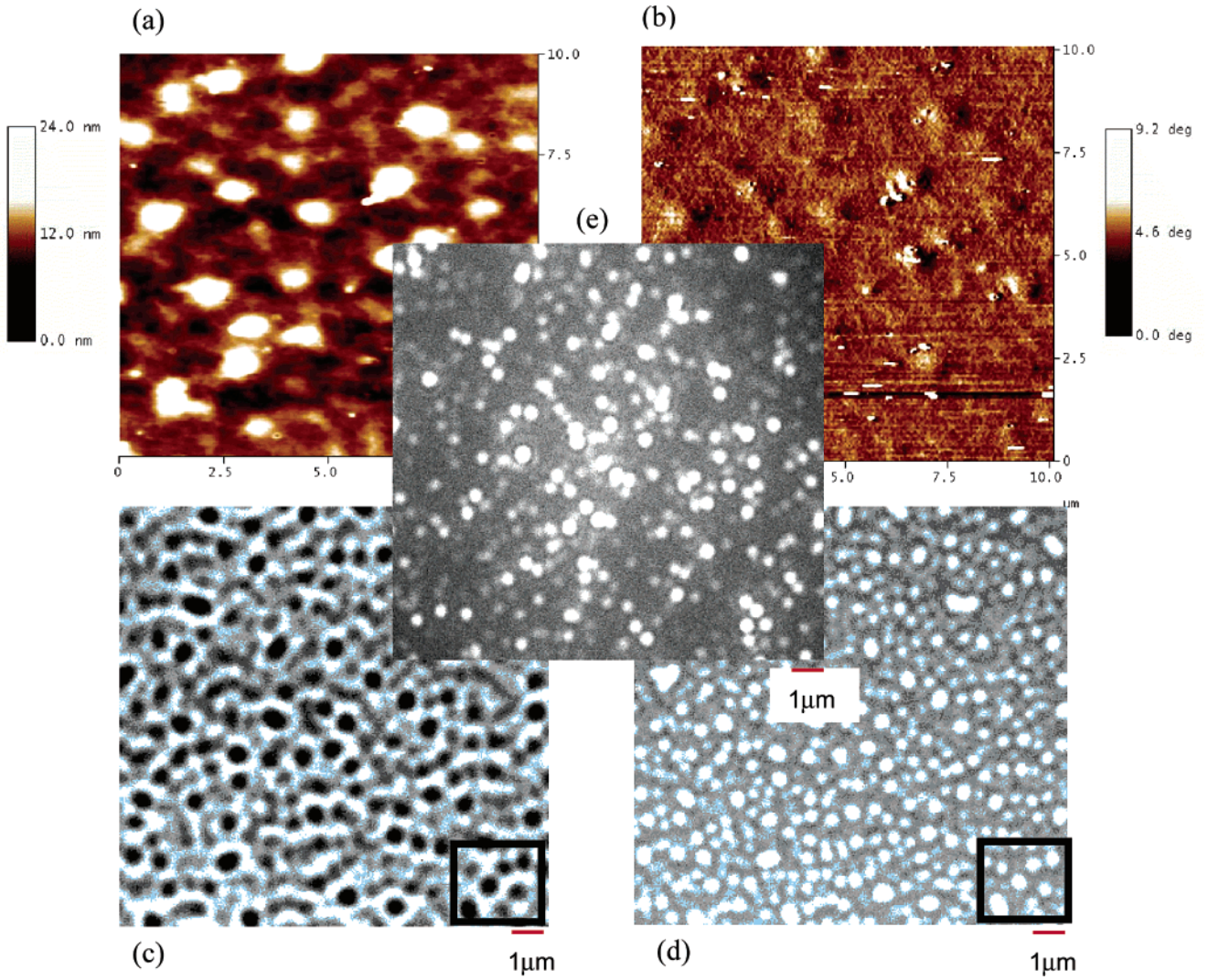

Figure 4. Images of 25 wt % MEH-PPV in PMMA: tapping mode AFM topographic (a) and phase (b) images; bright field (c) and photoluminescence (d) microscope images; (e) electroluminescence microscope image.

blend system. The phase image further demonstrates the difference in the surface topology due to the two different polymers present. Generally speaking, the phase image can provide details differentiating between different materials in a composite system. Further, it can help elucidate morphological features that are not resolved in a height image as evident by the results of Figure 3b. The morphology could also be observed through both bright field and fluorescence microscopy as shown in Figure 3c,d. The MEH-PPV domains appear as dark domains when observed under bright field illumination. Upon excitation with blue-violet light (425 nm band-pass ± 40 nm) and observation using a red transmitting (630 nm band-pass ± 60 nm) filter, these dark regions fluoresce, confirming the phase-separated domain morphology observed by AFM. The corresponding LED was made by spin-coating the 10 wt % blend solution on PEDOT-PSS coated ITO followed by drying the sample and thermal evaporation of 5 nm Ca and 200 nm Al as electrodes. Emission was observed from the devices (while applying an 8 V bias) through the fluorescence microscope, and the resulting image is shown in Figure 3e. It is immediately evident that this EL device shows light-emitting domains of MEH-PPV with submicron size. As the film is ~100 nm thick, each of these "nano"- or "micro"-LEDs can be envisioned as a separate small light source.

As the concentration of MEH-PPV is increased to 25 wt % in the blend, the phase-separated MEH-PPV domains at the surface of the film increase further in size to the micron range as shown by the AFM images in Figure 4a,b. This size expansion is not as evident in the optical, fluorescence, and the EL images in Figure 4c−e. At this concentration, it is interesting to note that the AFM, which is monitoring the surface topology, provides a somewhat different image than the optical and photoluminescence images. The AFM is able to discern how the MEH-PPV tends to pull up off the surface to provide the high features. Studying the optical images (Figure 4c,d), the entire content of the MEH-PPV domains is visible, which demonstrates that not all of the MEH-PPV has risen above the PMMA matrix. One possibility, as illustrated in Scheme 1, is that the MEH-PPV blooms over the top of the underlying PMMA, and the diameter of the bloom is about 20% larger than the size of the MEH-PPV domain at the electrode contact surface. As the PL, EL, and optical images probe the full thickness of the domain, the size expansion is not evident.

A close comparison of the bright-field and PL images is provided by studying the domains marked within the

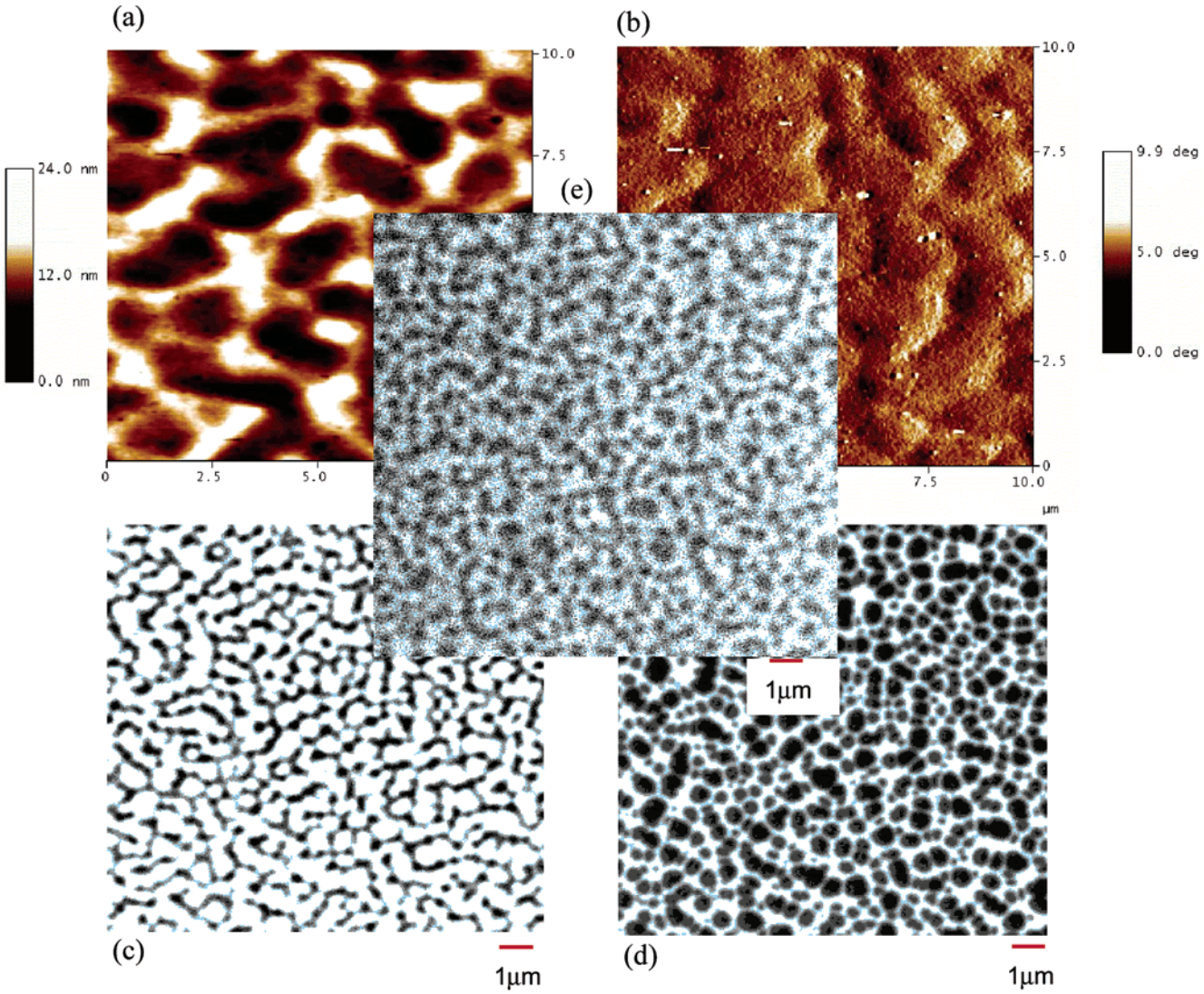

Figure 5. Images of 50 wt % MEH-PPV in PMMA: tapping mode AFM topographic (a) and phase (b) images; bright field (c) and photoluminescence (d) microscope images; (e) electroluminescence microscope image.

small box in the lower right-hand corner of each image of Figure 4c,d. This comparison is possible because the sample is not moved in the fluorescence microscope as images are recorded with both techniques. It can be seen that there is, as expected, a one-to-one correspondence between the dark MEH-PPV domains seen visibly with their PL response. The EL images also show similar topology.

A further increase in the MEH-PPV concentration to 50 wt % leads to a bicontinuous network as shown by the results of Figure 5. Examining the AFM images (Figure 5a,b), the isolated MEH-PPV domains, which were protruding from the surface at lower concentration, coalesce, leading to the network. The corresponding bright field, fluorescence, and EL micrographs show a similar bicontinuous morphology (Figure 5c−e). Inspecting the bright field and PL images, it initially seems as if the MEH-PPV is encompassing less than 50% of the surface area of the film. The difference between the EL and PL images in Figure 5 can be explained by the fact that the PL and EL experiments were done under different conditions. While obtaining the EL images, the light passes through the ITO coated glass (0.1−0.2 mm thick) and hence the focusing ability is reduced, which along with reflected light causes the EL image to appear more diffuse than the PL image. On the contrary, the PL image is obtained by exciting the polymer film through a thin glass cover and imaging the fluorescence. Further, it is possible that there is some mixing of the polymers, or as described earlier, complications due to layering or overlaying of the two materials may be occurring. This may provide at least one reason why the resultant EL image (Figure 5e) is more diffuse than the emitting domains shown in Figures 3 and 4.

At 75 wt % of MEH-PPV the morphology becomes fully inverted, evolving to a continuous raised MEH-PPV with an array of nonfluorescing PMMA domains illustrated by AFM in Figure 6a,b. These PMMA repressions in the film are about 1−2 μm in diameter. The bicontinuous morphology is not especially clear in the bright field, PL, or EL images (Figure 6c−e). Certain areas are dark upon observing PL and EL emission corresponding to regions where little or no MEH-PPV is present. Because of the high content of the MEH-PPV in the blend, it is difficult to discern the "light-emitting-only" regions, as was easily seen with lower MEH-PPV compositions.

Here we have shown a complete evolution of morphology as the content of conjugated polymer (MEH-PPV) is increased in the blend. The range of features observed with the variation of composition indicates that the two polymers are, as expected, incompatible. This evolution

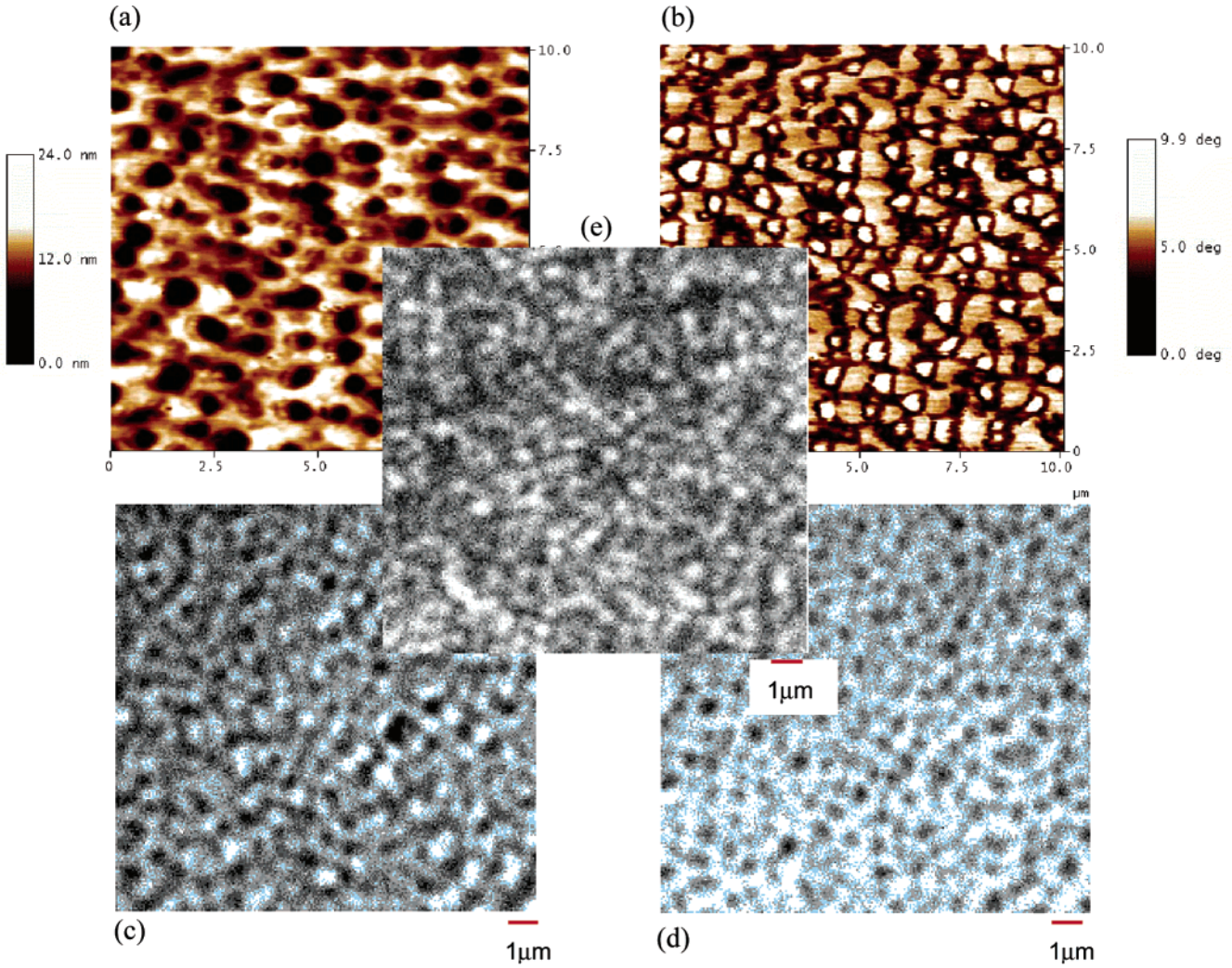

Figure 6. Images of 75 wt % MEH-PPV in PMMA: tapping mode AFM topographic (a) and phase (b) images; bright field (c) and photoluminescence (d) microscope images; (e) electroluminescence microscope image.

of structure has also been studied in cases of nonconjugated polymer blends including PMMA/PS[43]and deuterated polystyrene−polybromostyrene blend systems.[44] Since dichloroethane is a rapidly evaporating solvent, the morphology sets in during spin-coating in a nonequilibrium process. MEH-PPV has a lower surface energy than PMMA and tends to bloom to the surface as shown in Scheme 1. As the concentration of MEH-PPV is increased, the domains tend to intermix leading to a bicontinuous morphology. It is seen that the height of the topography remains constant at 24 nm and features higher than that are not observed.

PLED Device Characteristics. The light-emitting devices imaged in Figures 3e, 4e, 5e, and 6e contain as their active material the MEH-PPV/PMMA blends sandwiched between an ITO/PEDOT/PSS anode and a Ca/Al cathode. To characterize the performance of these materials in EL devices, current density−voltage ($J-V$) plots were measured for devices that contain all of the various blend compositions, and external quantum efficiencies as a function of drive voltage were compared for devices that contain 75 and 100 wt % MEH-PPV.

Figure 7a compares the $J-V$ plots for devices that contain the five different blends Two features are clearly apparent from these data: (1) the turn-on voltage for the devices systematically increases as the wt % of MEH-PPV in the blends decreases, and (2) the overall current density at a fixed voltage decreases with decreasing amount of MEH-PPV in the blend. The first feature indicates that the barrier to electron (or hole) injection increases with the amount of PMMA in the blend. This effect may arise due to selective adsorption of the insulating phase (PMMA) at one of the electrode interfaces. The second observation, that the overall current density at fixed voltage increases with wt % MEH-PPV, indicates that the overall resistance of the polymer film decreases as the amount of MEH-PPV in the blend increases. Given that MEH-PPV is active as the charge transport material in the films and provides a connection between the anode and cathode, it is quite reasonable to expect that the overall film resistance should be approximately proportional to the amount of MEH-PPV in the blends. Close inspection of the $J-V$ data reveals that this is approximately correct. For example, the device that contains the 50% blend passes only slightly less than 50% of the current passed by pure MEH-PPV. Thus, the conductivity of the MEH-PPV phase in the blends remains relatively constant, and the overall current passed by the blend devices decreases because the effective area available for charge transport through the films decreases with the wt % of MEH-PPV. This result indicates that for a fixed voltage the current density within the MEH-PPV phase remains relatively

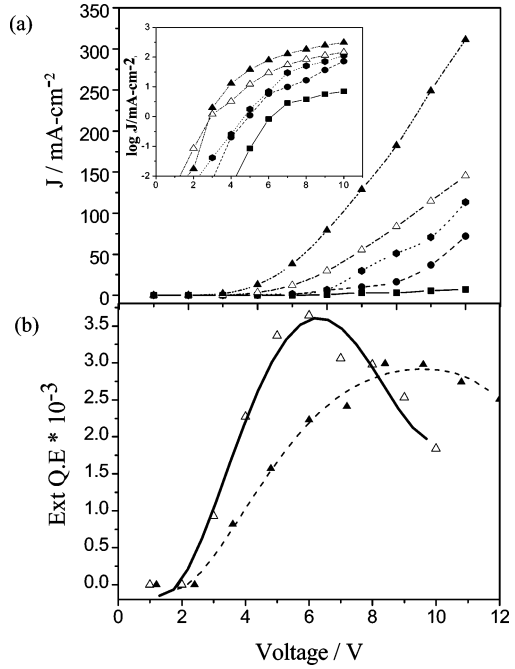

Figure 7. (a) Current density−voltage plot ($J-V$) for the blend devices and MEH-PPV. Inset shows log J vs applied voltage. (b) Comparison of external quantum efficiencies of 75 wt % blend and MEH-PPV. Legend: (■) 10% MEH-PPV; (●) 25% MEH-PPV; (⬢) 50% MEH-PPV; (△) 75% MEH-PPV; (▲) 100% MEH-PPV.

constant even though the composition of the blends varies.

In a more limited investigation, we compared the external quantum efficiency as a function of drive voltage for devices that contain 75 and 100 wt % MEH-PPV, and the results are plotted in Figure 7b. These results were obtained by averaging three devices, and the values were within 10% of each other. The results indicate that the peak efficiency of the 75 wt % MEH-PPV device is approximately 20% higher than that of the device that contains pure MEH-PPV. In addition, the peak efficiency for the 75 wt % blend device occurs at a lower drive voltage. Although it is difficult to draw definitive conclusions on the basis of these preliminary results, we can make several proposals as to possible origins of the modest increase in efficiency with decrease in wt % MEH-PPV in the devices. First, because of the phase segregation in the MEH-PPV/PMMA blends, the charge carriers are confined to the MEH-PPV domains. The phase segregation may lead not only to spatial confinement but also to the production of carrier trap sites (e.g., at MEH-PPV/PMMA interfaces). The net result of the spatial confinement and carrier trapping may be to induce a net increase in the electron−hole pair recombination efficiency, which increases the operating efficiency of the device. Another possible origin of increased efficiency in the blend devices may arise due to the effect of the phase segregation on the surface morphology of the blends. Specifically, as shown in the AFM topographic images, the MEH-PPV domains are elevated above the mean surface of the film. This surface elevation may improve the quality of the interface between the MEH-PPV domains and the Ca/Al cathode, resulting in an increased efficiency for electron injection. Since the overall efficiency of the devices is relatively low (presumably because of a higher efficiency for hole injection at the anode), any improvement in electron injection at the cathode/film interface is expected to lead to an overall increase in device efficiency. Another possibility is that at 75% MEH-PPV the chains are more isolated from each other when compared to 100% MEH-PPV, which can lead to reduction in self-quenching leading to increased device efficiency.

Summary and Conclusions

The evolution of the morphology of thin films consisting of blends of MEH-PPV and PMMA has been characterized by AFM and bright field and fluorescence microscopy. The films exhibit a phase-segregated structure that is characterized by domains with length scales ranging from 200 to 900 nm. The nanostructure of the blends is strongly dependent on the composition, and consequently the morphology can be tuned according to the particular requirements of a given electrooptical application. Electroluminescent devices fabricated with blends in which MEH-PPV is the minority phase feature emission from individual "dots" having apparent diameters of 200−500 nm. In a limited study of the electroluminescence efficiency as a function of blend composition, it was found that the efficiency was moderately higher in devices fabricated with 75 wt % MEH-PPV compared to a device that contained pure MEH-PPV in the active layer. Further investigations concerning the relationships between device characteristics, electron-to-photon quantum efficiency, blend composition, morphology, and the nature of the emitting and the nonconjugated polymer materials are presently underway in our laboratories. The results of this work will be described in the near future.

Experimental Details

PMMA (M_w = 82 kDa) was purchased from Aldrich and was used as received. MEH-PPV (M_w = 38 kDa) was purchased from H.W. Shands and was used as received. The individual polymer solutions were prepared by dissolving the homopolymers in 1,2-dichloroethane at a concentration of 5.2 mg/mL. Polymer blend solutions were prepared by mixing the corresponding homopolymer solutions to obtain the required composition.

Glass substrates (Corning coverglass, 25 mm^2) were used for AFM, optical, and fluorescence measurements. They were first spin-coated with PEDOT-PSS (Bayer Baytron P VP Al 4083) at 4000 rpm and dried under vacuum for 2 h at 150 °C. The polymer blend films were prepared by spin-coating at 1000 rpm for 30 s. Thickness measurements were made with a Dektak 3030 profilometer over several points of each sample to yield an average thickness of 100−120 nm on all films.

Tapping mode AFM was carried out using a Nanoscope IIIa Dimension 3100. Optical and fluorescence microscopy images were taken using an Olympus IX70 fitted with a 100 W Hg source (USH-102DH) and a CCD camera (Princeton, RTE 1300 × 1030) mounted on the side port. Fluorescence microscopy was carried out with a blue-violet modular filter cube (Chroma Technology, excitation 425 nm, 40 nm band-pass; emission 630 nm, 60 nm band-pass; 475 nm dichroic splitter). Fluorescence images were collected through 10× and 40× objective lenses (Olympus U Plan Fl, 0.30NA and SLC Plan Fl, 0.55NA, respectively). For obtaining the fluorescence images a blue-violet filter (425 nm band-pass ± 40 nm) was used to filter the excitation source, and a red filter (630 nm band-pass ± 60 nm) was used to filter the emission light.

Electroluminescent devices were prepared by etching masked ITO glass (Delta Technologies, R_s = 8−12 Ω) by exposure to aqua regia vapor. The etched substrate was cleaned in an ultrasonic bath with aqueous sodium dodecyl sulfate (SDS) (Fisher, Versa-Clean solution), Milli-Q water, acetone, and 2-propanol. This was followed by spin-coating with PEDOT/

PSS and drying as described above. The polymer blend solutions were then spin-coated, and the resulting films were dried under vacuum (1×10^{-6} Torr) for 12 h at room temperature. Calcium (50 Å) and aluminum (2000 Å) were sequentially deposited by thermal evaporation on the polymer film. After deposition, the devices were encapsulated with epoxy under an Ar atmosphere in order to minimize exposure to air and oxygen. All device measurements were carried out at room temperature. The active area on the etched ITO was 0.07 cm^2. Spectral measurements were carried out on an ISA-SPEX Triax 180 spectrograph fitted with a liquid N_2 cooled CCD detector (EEV back-illuminated CCD, 1024 × 128 pixels, 400−1100 nm). A secondary standard tungsten lamp was used to calibrate the CCD detector. Measurements were made normal to the surface of the devices, and in the computation of EL quantum efficiencies it was assumed that the spatial distribution was Lambertian.[45] External device quantum efficiencies were calculated as described in the literature.[46] The images of the devices were taken using 10× and 40× objective lenses in the fluorescence microscope while being powered by a Keithley 228 voltage−current source.

Acknowledgment. We gratefully acknowledge funding from the Defense Advanced Research Projects Agency (Grant DAAD 19-00-1-0002) and the DOE-BES.

References and Notes

(1) Burroughes, J. H.; Bradley, D. D. C.; Brown, A. R.; Marks, R. N.; Mackay, K.; Friend, R. H.; Burns, P. L.; Holmes, A. B. *Nature (London)* **1990**, *347*, 539.
(2) Braun, D.; Heeger, A. J. *Appl. Phys. Lett.* **1991**, *58*, 1982.
(3) Kraft, A.; Grimsdale, A. C.; Holmes, A. B. *Angew. Chem., Int. Ed.* **1998**, *37*, 402.
(4) Friend, R. H.; Gymer, R. W.; Holmes, A. B.; Burroughes, J. H.; Marks, R. N.; Taliani, C.; Bradley, D. D. C.; Dos Santos, D. A.; Brédas, J. L.; Lögdlund, M.; Salaneck, W. R. *Nature (London)* **1999**, *397*, 121.
(5) Dai, L.; Winkler, B.; Dong, L.; Tong, L.; Mau, A. W. H. *Adv. Mater.* **2001**, *13*, 915.
(6) Morgado, J.; Cacialli, F.; Friend, R. H.; Chuah, B. S.; Rost, H.; Moratti, S. C.; Holmes, A. B. *Synth. Met.* **2001**, *119*, 595.
(7) Sarker, A. M.; Gürel, E. E.; Ding, L.; Styche, E.; Lahti, P. M.; Karasz, F. E. *Synth. Met.* **2003**, *132*, 227.
(8) Burn, P. L.; Kraft, A.; Baigent, D. R.; Bradley, D. D. C.; Brown, A. R.; Friend, R. H.; Gymer, R. W.; Holmes, A. B.; Jackson, R. W. *J. Am. Chem. Soc.* **1993**, *115*, 10117.
(9) Zheng, M.; Ding, L.; Gürel, E. E.; Lahti, P. M.; Karasz, F. E. *Macromolecules* **2001**, *34*, 4124.
(10) Kim, H. W.; Ryu, M. K.; Kim, K. D.; Lee, S. M. *Macromolecules* **1998**, *31*, 1114.
(11) Herrema, J. K.; Hutten van, P. F.; Gill, R. E.; Wildeman, J.; Wieringa, R. H.; Hadziioannou, G. *Macromolecules* **1995**, *28*, 8102.
(12) Hilberer, A.; Brouwer, H. J.; Scheer van der, B. J.; Wildeman, J.; Hadziioannou, G. *Macromolecules* **1995**, *28*, 4525.
(13) Hochfilzer, C.; Tasch, S.; Winkler, B.; Huslage, J.; Leising, G. *Synth. Met.* **1997**, *85*, 1271.
(14) Morgado, J.; Cacialli, F.; Friend, R. H.; Chuah, B. S.; Rost, H.; Holmes, A. B. *Macromolecules* **2001**, *34*, 3094.
(15) Brouwer, H. J.; Hilberer, A.; Krasnikov, V. V.; Werts, M.; Wildeman, J.; Hadziioannou, G. *Synth. Met.* **1997**, *84*, 881.
(16) Granström, M.; Inganäs, O. *Adv. Mater.* **1995**, *7*, 1012.
(17) Granström, M.; Berggren, M.; Inganäs, O. *Science* **1995**, *267*, 1479.
(18) He, G.; Li, Y.; Liu, J.; Yang, Y. *Appl. Phys. Lett.* **2002**, *80*, 4247.
(19) Blumstengel, S.; Sokolik, I.; Dorsinville, R.; Voloschenko, D.; He, M.; Lavrentovich, O.; Chein, L. C. *Synth. Met.* **1999**, *99*, 85.
(20) Nishino, H.; Yu, G.; Heeger, A. J.; Chen, T. A.; Rieke, R. D. *Synth. Met.* **1995**, *68*, 243.
(21) Berggren, M.; Inganäs, O.; Gustafsson, G.; Rasmusson, J.; Andersson, M. R.; Hjertberg, T.; Wennerstörm, O. *Nature (London)* **1994**, *372*, 444.
(22) Granström, M.; Berggren, M.; Inganäs, O.; Andersson, M. R.; Hjertberg, T.; Wennerstörm, O. *Synth. Met.* **1997**, *85*, 1193.
(23) Granström, M.; Inganäs, O. *Appl. Phys. Lett.* **1996**, *68*, 147.
(24) List, E. J. W.; Graupner, W.; Wohlgenannt, M.; Leising, G.; Partee, J.; Shinar, J.; Schlichting, P.; Rohr, U.; Geerts, Y.; Scherf, U.; Mullen, K. *Opt. Lett.* **1998**, *9*, 494.
(25) Palilis, L. C.; Lidzey, D. G.; Redecker, M.; Bradley, D. D. C.; Inbasekaran, M.; Woo, E. P.; Wu, W. W. *Synth. Met.* **2000**, *111−112*, 159.
(26) Granström, M.; Berggren, M.; Pede, D.; Inganäs, O.; Andersson, M. R.; Hjertberg, T.; Wennerstörm, O. *Supramol. Sci.* **1997**, *4*, 27.
(27) Yang, C. Y.; Hide, A. J.; Heeger, A. J.; Cao, Y. *Synth. Met.* **1997**, *84*, 895.
(28) Morgado, J.; Friend, R. H.; Cacialli, F.; Chuah, B. S.; Moratti, S. C.; Holmes, A. B. *J. Appl. Phys.* **1999**, *86*, 6392.
(29) He, G.; Liu, J.; Li, Y.; Yang, Y. *Appl. Phys. Lett.* **2002**, *80*, 1891.
(30) Cui, H.; Lee, H. *Synth. Met.* **2001**, *117*, 255.
(31) Han, H. J.; Lee, Y. S.; Nahm, K. S.; Cho, E. H.; Ko, S. B.; Kim, C. J.; Jeon, I. C.; Lee, W. H.; Suh, E. K.; Lee, Y. H. *Bull. Korean Chem. Soc.* **1999**, *20*, 1093.
(32) Ding, L.; Karasz, F. E.; Lin, Z.; Zheng, M.; Liao, L.; Pang, Y. *Macromolecules* **2001**, *34*, 9183.
(33) Lee, J.; Kang, I.; Hwang, D.; Shim, H.; Jeoung, S. C.; Kim, D. *Chem. Mater.* **1996**, *8*, 1925.
(34) Hsu, J. H.; Kuen, P. K.; Fann, W.; Chuang, K. R.; Chen, S. A. *J. Appl. Phys.* **1998**, *83*, 1782.
(35) Morgado, J.; Moons, E.; Friend, R. H.; Cacialli, F. *Synth. Met.* **2001**, *124*, 63.
(36) Arias, A. C.; MacKenzie, J. D.; Stevenson, R.; Halls, J. J. M.; Inbasekaran, M.; Woo, E. P.; Richards, D.; Friend, R. H. *Macromolecules* **2001**, *34*, 6005.
(37) Corcoran, N.; Arias, A. C.; Kim, J. S.; MacKenzie, J. D.; Friend, R. H. *Appl. Phys. Lett.* **2003**, *82*, 299.
(38) Kulkarni, A. P.; Jenekhe, S. A. *Macromolecules* **2003**, *36*, 3686.
(39) Chao, C. S.; Whang, W. T.; Chuang, K. R. *J. Polym. Res.* **2000**, *7*, 175.
(40) Chihaya, A.; Seiji, H.; Toshiki, K.; Yoshio, T. *Jpn. J. Appl. Phys., Part 2: Lett.* **1997**, *36*, L827−L830.
(41) Buschbaum, P. M.; Stamm, M. *Macromolecules* **1998**, *31*, 3686.
(42) Affrossman, S.; O'Neill, S. A.; Stamm, M. *Macromolecules* **1998**, *31*, 6280.
(43) Walheim, S.; Böltau, M.; Mlynek, J.; Krausch, G.; Steiner, U. *Macromolecules* **1997**, *30*, 4995.
(44) Affrossman, S.; Henn, G.; O'Neill, S. A.; Pethrick, R. A.; Stamm, M. *Macromolecules* **1996**, *29*, 5010.
(45) Greenham, N. C.; Friend, R. H.; Bradley, D. D. C. *Adv. Mater.* **1994**, *6*, 491.
(46) He, Y.; Hattori, R.; Kanicki, J. *Rev. Sci. Instrum.* **2000**, *71*, 2104.

MA034908W